

# Simulation of resist reflow with non-uniform viscosity profile

F Sidorov, A Rogozhin

Valiev Institute of Physics and Technology, Russian Academy of Sciences, Moscow,  
117218 Russia

E-mail: [sidorov@ftian.ru](mailto:sidorov@ftian.ru)

**Abstract.** This paper proposes a new approach to simulation of e-beam exposed PMMA thermal viscoelastic reflow taking into account its non-uniform viscosity profile. The developed algorithm employs numerical “soapfilm” modeling of PMMA surface evolution, processed by free software “Surface Evolver” in area normalization mode. PMMA viscosity profile after exposure is determined by Monte-Carlo simulation of PMMA main-chain scissions and kinetic equations, describing PMMA molecular weight distribution changes. Vertex mobilities of PMMA surface were determined by simulation of uniform rectangular gratings thermal reflow using both analytical and numerical approaches in wide viscosity range. The agreement between reflowed profiles simulated by these two approaches is obtained, which emphasizes the applicability of soapfilm modeling to simulation of polymer thermal reflow. The inverse mobility of PMMA surface vertices appeared to be proportional to PMMA viscosity with high accuracy. The developed algorithm enables simulation of complex non-uniform structures reflow, which leads to better understanding of thermal reflow processes and can be applied for predictable reflow usage as a stage of 3D microfabrication.

*Keywords:* e-beam lithography, resist depolymerization, thermal reflow

## 1. Introduction

Thermal reflow processes can modify initial polymer resist profile significantly, provided its viscosity, and this phenomenon has its advantages and disadvantages. For example, thermal reflow is applied as a stage of microstructuring for smoothing of the relief obtained by grayscale e-beam lithography [1] or nanoimprint lithography [2], which allows one to obtain various 3D structures. On the other hand, resist profile deformation by thermal reflow reduces profile aspect ratio, which is undesirable in certain cases. Thermal reflow can also affect structures obtained by standard “wet” e-beam lithography process. E-beam exposure and proximity effects lead to molecular weight reduction of the whole resist layer, which stimulates resist reflow at post-exposure and post-develop bake stages. Taking into account all this effects the method allowing exact determination of reflow processes influence on resulting structure profile in any specific processes is highly desirable.

Two common approaches to simulation of resist thermal reflow could be distinguished. The first include analytical methods based on transfer equations. For instance, Leveder et al. used an analytical spectral method to simulate the reflow of isodense periodic structures with various periods [3, 4, 5]. This method is based on 2D Navier-Stokes equation coupled to continuity equation with the assumption of no slip length and no Marangoni effect but considering Laplace pressure and Hamaker energy. In this algorithm the initial structure profile is Fourier transformed and then reflow process is simulated by decay of profile harmonics:

$$h(x, t) = h_0 + \tilde{h}(x, t), \quad (1)$$

$$\tilde{h}(x, t) = \sum_{-\infty}^{+\infty} a_n(0) \exp\left(-\frac{t}{\tau_n} + i n \frac{2\pi}{\lambda} x\right), \quad (2)$$

$$\tau_n = \frac{3\eta}{\gamma h_0^3} \times \left(\frac{\lambda}{2\pi n}\right)^4. \quad (3)$$

where  $\lambda$  – profile spatial periodicity,  $\eta$ ,  $\gamma$  – polymer viscosity and surface tension, respectively,  $a_n(0)$  – Fourier coefficients of initial polymer profile,  $h_0$  – polymer layer thickness. Polymer viscosity depends both on temperature and polymer molecular weight, which should be taken into account in simulation. Temperature dependence of viscosity could be described by Williams–Landel–Ferry (WLF) equation [6]:

$$\log\left(\frac{\eta(T)}{\eta(T_0)}\right) = -\frac{C_1(T - T_0)}{C_2 + (T - T_0)}, \quad (4)$$

which parameters  $\eta(T_0)$ ,  $C_1$ ,  $C_2$  and  $T_0$  for three different resists are provided in Table 1 [7].

**Table 1.** Parameters of equation 4, obtained by Aho et al. for polystyrene 143E by BASF (PS), poly(methyl methacrylate) Plexiglas 6N by Degussa (PMMA) and polycarbonate Lexan HF1110R by GE Plastics (PC) [7].

Parameter	PS	PMMA	PC
$\eta(T_0)$ , Pa · s	7310.4	13450	2763
$C_1$	10.768	7.6682	4.7501
$C_2$ , °C	289.21	210.76	110.12
$T_0$ , °C	190	200	200

Withal, the dependence of polymer viscosity on its molecular weight could be described by empirical formula:

$$\eta \propto M_n^\alpha, \quad (5)$$

where  $M_n$  – number average polymer molecular weight. For PMMA  $\alpha$  comprises 3.4 at  $M_n \geq 48000$  and 1.4 at  $M_n < 48000$  [4, 8]. Equations (4, 5) allow one to calculate polymer viscosity for different temperatures and molecular weights (Fig. 1).

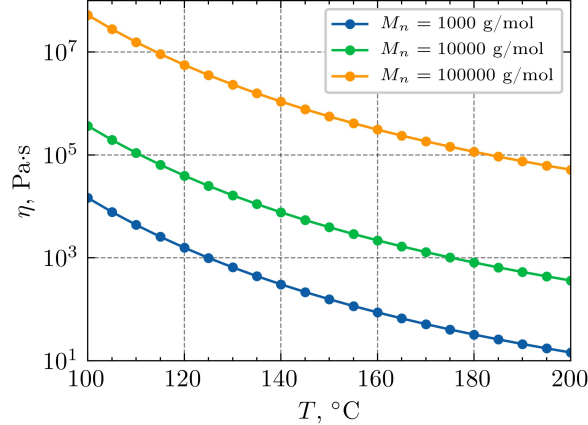


**Figure 1.** Temperature viscosity dependencies for PMMA with different number average molecular weights, obtained by equations (4, 5).

The accuracy of this analytical method is quite high for the simulation of polymer reflow at  $a_n(t) \ll h_0$ , however, it couldn't be applied in case of non-uniform polymer viscosity profile.

The second approach, numerical one, is based on search of minimal surface by finite elements method. It can be processed by free software “Surface Evolver” (SE) – the program for the modelling of liquid surfaces shaped by various forces and constraints [9]. SE allows a wide spectrum of possible energies to be assigned like gravitational energy, surface energy, and further different implementations of mean and Gaussian curvature. For the purpose of polymer reflow simulation only surface energy should be taken into account.

In SE simulation algorithm the structure is only described by its “outer shell” (soapfilm modeling) (Fig. 2a)). For the resist reflow simulation the resist surface is divided into triangle facets defined by vertices  $v_0$ ,  $v_1$  and  $v_2$  and oriented edges  $\vec{e}_0$ ,  $\vec{e}_1$  and  $\vec{e}_2$ , and the polymer reflow is simulated by moving of facet vertices, maintaining the constant volume inside the surface. The force on vertex  $v_0$  (the tail of vector  $\vec{e}_0$ ) is

$$\vec{F}_{v_0} = \frac{\gamma_i}{2} \cdot \frac{\vec{e}_1 \times (\vec{e}_0 \times \vec{e}_1)}{\|\vec{e}_0 \times \vec{e}_1\|}, \quad (6)$$

where  $\gamma_i$  – is surface tension of  $i$ -th facet (Fig. 2b)). SE could be operated in the area normalization mode to approximate a vertex motion by mean curvature, i.e., a surface tension flow. In this mode, the velocity of a vertex is proportional to force and indirectly proportional to the area of the facets surrounding this vertex. The  $i$ -th facet has three vertices associated with it, therefore the relative area contribution to the force of one vertex is  $1/3$  the area of the surrounding facets  $A$ . The vertex velocity in the area normalization mode is

$$\vec{v} = \frac{\vec{F}}{A/3} \cdot \mu, \quad (7)$$

where  $\mu$  is so called vertex mobility. The vector of vertex movement  $\vec{\delta}$  is then calculated

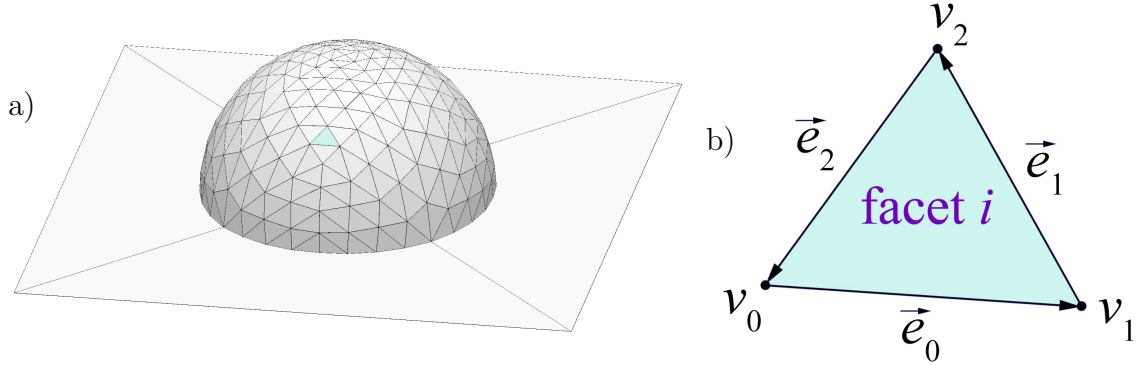


**Figure 2.** a) A mound of liquid sitting on a tabletop with gravity acting on it, defined by its surface in SE, b) definition of vertices and oriented edges for  $i$ -th facet in SE.

as product of vertex velocity and *scale* factor  $s$ , the physical representation of simulation step time:

$$\vec{\delta} = \vec{v} \cdot s. \quad (8)$$

In most cases SE is used just for calculation of minimal energy geometries, which doesn't imply simulation of liquid or polymer flow dynamics [10, 11]. However, Kirchner [12, 13] demonstrated the applicability of this method for the reflow simulation of step structure, which consisted of two regions with different molecular weight. The difference in viscosity values of regions was taken into account by setting different vertex mobilities. Kirchner showed that mobility ratios 1:2, 1:5 and 1:50 allow to describe structure reflow stages with high accuracy. Mobility ratios were determined empirically, by the comparison of experimental and simulated profiles. In this case, the simulation algorithm is only applicable for the structures obtained with the same exposure doses, and reflow simulation of any other structures require preliminary measurements. On the other hand, the only question in case of any structure reflow simulation operated by SE is the distribution of structure vertex mobilities (neglecting the edge effects). Kirchner mentioned that inverse mobility is a kind of sample viscosity, but the correlation between mobility and viscosity was still unclear. Thus, the purpose of this study is to investigate the relation between polymer viscosity and mobility of its surface vertices and to develop the numerical simulation method for non-uniform resist reflow, using SE as a calculation engine.

## 2. Simulation of polymer viscosity distribution

In this study, simulation of exposer polymer resist viscosity distribution is based on Monte-Carlo simulation of e-beam scattering in PMMA. The algorithm described in [14] was used to simulate polymer main-chain scissions during the resist exposure in series of parallel lines. E-beam energy was 20 keV, exposure current – 3 nA per 1 cm of line, PMMA layer thickness – 500 nm, line pitch – 3  $\mu\text{m}$  (Fig. 3).

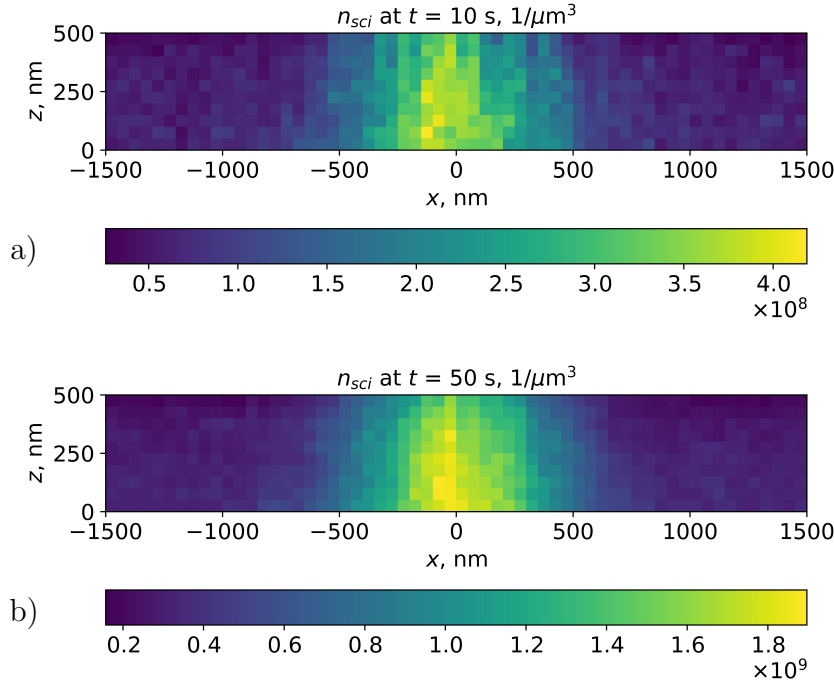


**Figure 3.** Simulation of scission distribution in PMMA layer, obtained by the model described in [14] for exposure in series of parallel lines at 130 °C. Line dose is around 3 nA/cm, e-beam energy is 20 keV, PMMA layer thickness – 500 nm, exposure time is 10 s (a) and 50 s (b).

Dividing line volume into 5 nm cells allowed to simulate depolymerization chain initiation constant in each cell (the number of scissions per monomer per 1 s). This constant was used for simulation of PMMA local molecular weight using approach described in [15, 16, 17]. It bases in the assumption of Schulz-Zimm polymer weight distribution [18]:

$$P_n = C_0 n^z \exp(-n/y) \quad (9)$$

where  $P_n$  – number of molecules with degree of polymerization equal to  $n$ ,  $C_0$  – normalization factor. Parameter  $z$  describes the width of distribution:

$$M_w/M_N = (z + 2)/(z + 1), \quad (10)$$

where  $M_n$  and  $M_w$  – number average and weight average molecular weight, respectively, parameter  $y$  is related to number average polymerization degree  $x$ :

$$x = y(z + 1). \quad (11)$$

In this case polymer degradation could be described by equation on polymer molecular weight moments:

$$\frac{dM_i}{dt} = k_s \left( \frac{2}{i+1} - 1 \right) M_{i+1} + \frac{dM_0}{dt} - k_s M_1 - \frac{i}{\gamma} \left( k_s M_i + \frac{dM_{i-1}}{dt} \right) \quad (i \geq 1), \quad (12)$$

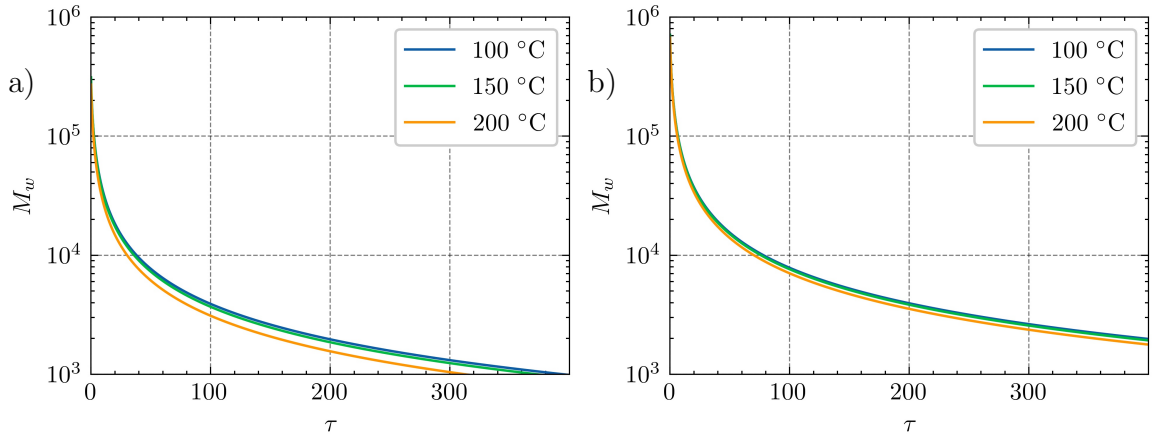


**Figure 4.**  $M_n$  and  $M_w$  dependence on  $\tau$  obtained by approach provided in [17].

where  $1/\gamma$  – average depolymerization zip length,  $M_i$  – moment of molecular weight distribution of  $i$ -th order:

$$M_i = \sum_{n=2}^{\infty} n^i P_n, \quad (13)$$

$k_s$  – depolymerization chain initiation constant. The result of PMMA molecular weight simulation for different exposure moments is shown in Fig. 5. Average depolymerization zip length could be obtained by exponential fit of values provided by Mita [19] for PMMA in case of depolymerization termination or chain transfer at the end of molecule.

Using the relation between  $M_i$ ,  $M_1$ ,  $y$  and  $z$ :

$$M_i = M_1 \prod_{n=2}^i (z + n)y^{i-1}, \quad (14)$$

one could describe Shultz-Zimm distribution parameter ( $C_0$ ,  $z$  and  $y$ ) changes by three equations of the form of (12) (see Appendix). This results in local  $M_n$  and  $M_w$  dependence on exposure time (Fig. 4), which allow to calculate local polymer viscosity distribution (Fig. 5).

### 3. Determination of polymer vertex mobility

Obtained polymer local viscosity distribution still could not be utilized for reflow simulation – the approach based on Fourier transform of profile requires uniform resist viscosity profile. On the other hand, the numerical approach bases on vertex mobilities, not viscosity. Therefore, one should introduce the correlation between polymer viscosity and vertex mobilities of its surface. For this purpose, the reflow of rectangular PMMA gratings was simulated by both approaches. Grating parameters corresponded to realistic values for NIL – 2  $\mu\text{m}$  pitch and 28 nm depth. The viscosity of PMMA varied in range  $10^2$ – $10^6$  Pa·s and for each viscosity value reflow process was simulated until grating depth decreased to values 1–2 nm in nearly same steps. Then the grating surface was reconstructed in SE program and surface evolution during grating reflow was simulated.

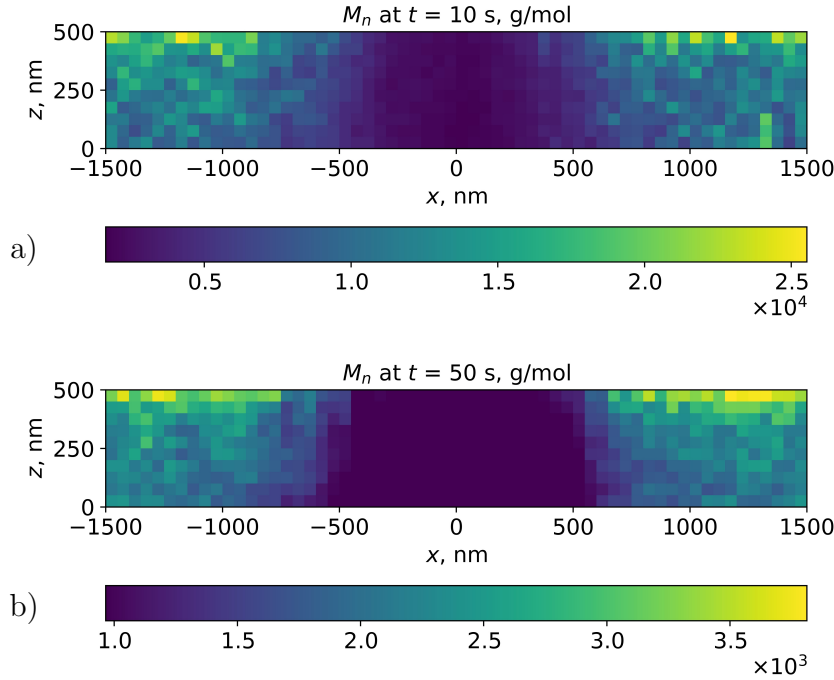


**Figure 5.** Simulation of PMMA molecular weight distribution during exposure in series of parallel lines. Line dose is around 3 nA/cm, e-beam energy is 20 keV, PMMA layer thickness – 500 nm, exposure time is 10 s (a) and 50 s (b).

During the surface evolution the *scale* values, giving the same surface shape as one obtained using analytical approach, were determined (Fig. 6). It was found that in the beginning of reflow there is slight discrepancy between profiles simulated by both approaches, but then both approaches lead to almost sinusoidal shape as it is predicted by formula 1.

Time-*scale* data obtained for each viscosity value showed almost linear dependence between *scale* and time:

$$\text{scale} \approx \alpha \cdot t. \quad (15)$$

Each time-*scale* data was fitted by linear function (Fig 7) which result in almost linear dependence of  $\ln(\alpha)$  on  $\ln(\eta)$  (Fig. 8). Taking into account the fact that  $\alpha$  is being multiplied by scale and this results in time, one could get the needed relation between polymer viscosity and mobility of its vertices:

$$\mu = C/\eta^\beta, \quad (16)$$

where  $C \approx 26.16$  and  $\beta \approx 0.989$ , which is an almost direct proportionality between inverse mobility of polymer surface vertices and polymer viscosity.

proportionality between polymer viscosity and mobility of its vertices. Therefore, one could convert nonuniform polymer viscosity distribution into distribution of polymer vertex mobilities, which could be embedded into SE simulation. Noteworthy, this approach seems to be reasonable in case of 1D and 2D viscosity distributions (when

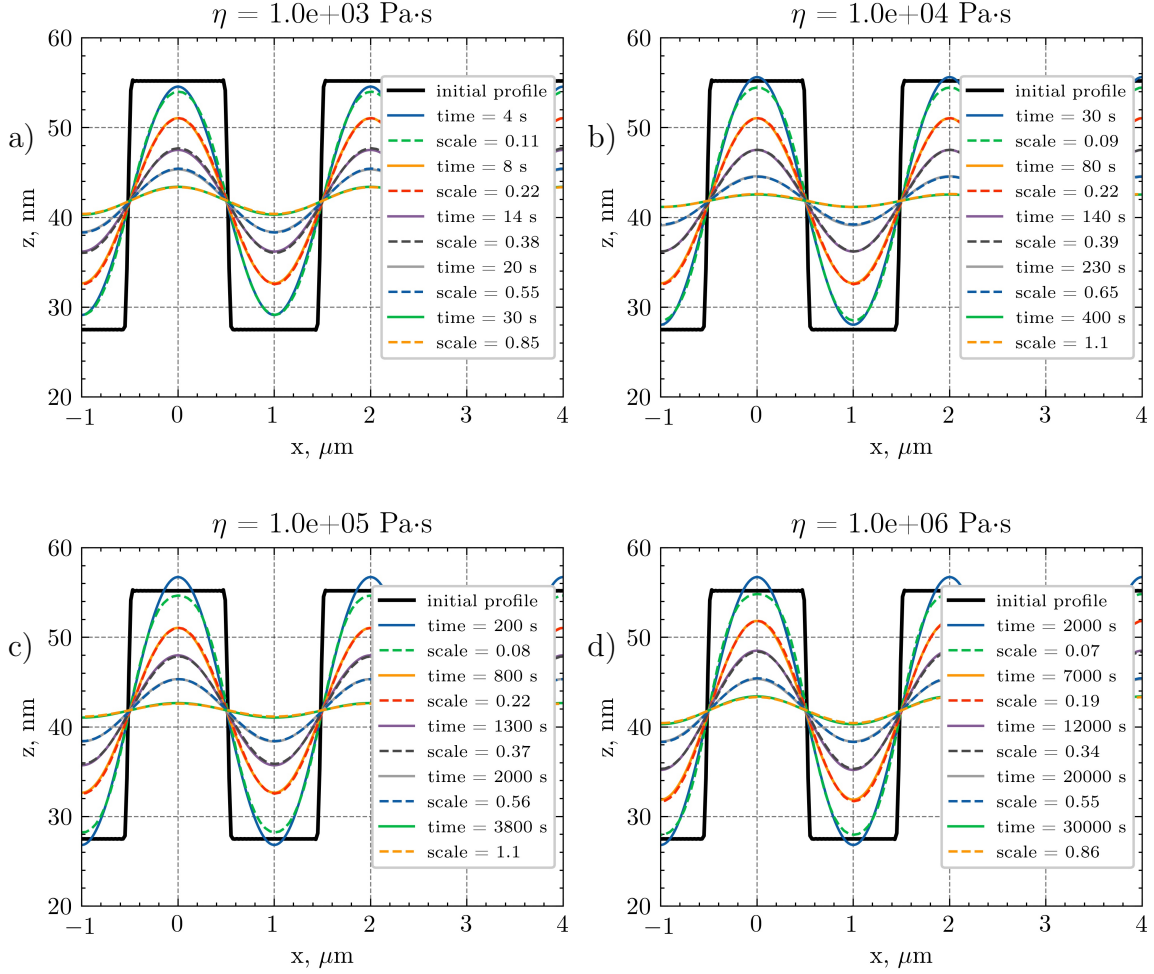


**Figure 6.** Reflow of rectangular grating simulated by analytical and numerical approaches for different viscosity values.

resist viscosity doesn't change along vertical direction). In case of 3D resist viscosity distribution polymer viscosity along vertical direction seem to have been averaged.

#### 4. Discussion

The developed method of polymer resist vertex mobility determination has several remarkable features. First, it demonstrates the agreement between reflowed profiles, simulated by analytical spectral method and ones obtained by numerical SE simulation in area normalization mode. This emphasizes the applicability of soapfilm modeling for the simulation of polymer reflow and confirms the linear relation between *scale* and time, proposed by Kirchner [12]. Moreover, the relation of inverse mobility and polymer viscosity appears to be also almost linear. It is also noteworthy that developed method brings clarity into SE reflow simulation process – in case of usage proper mobility values the *scale* factor denotes exactly the actual reflow time.

Second, this method could be applied for reflow simulation of any structure obtained

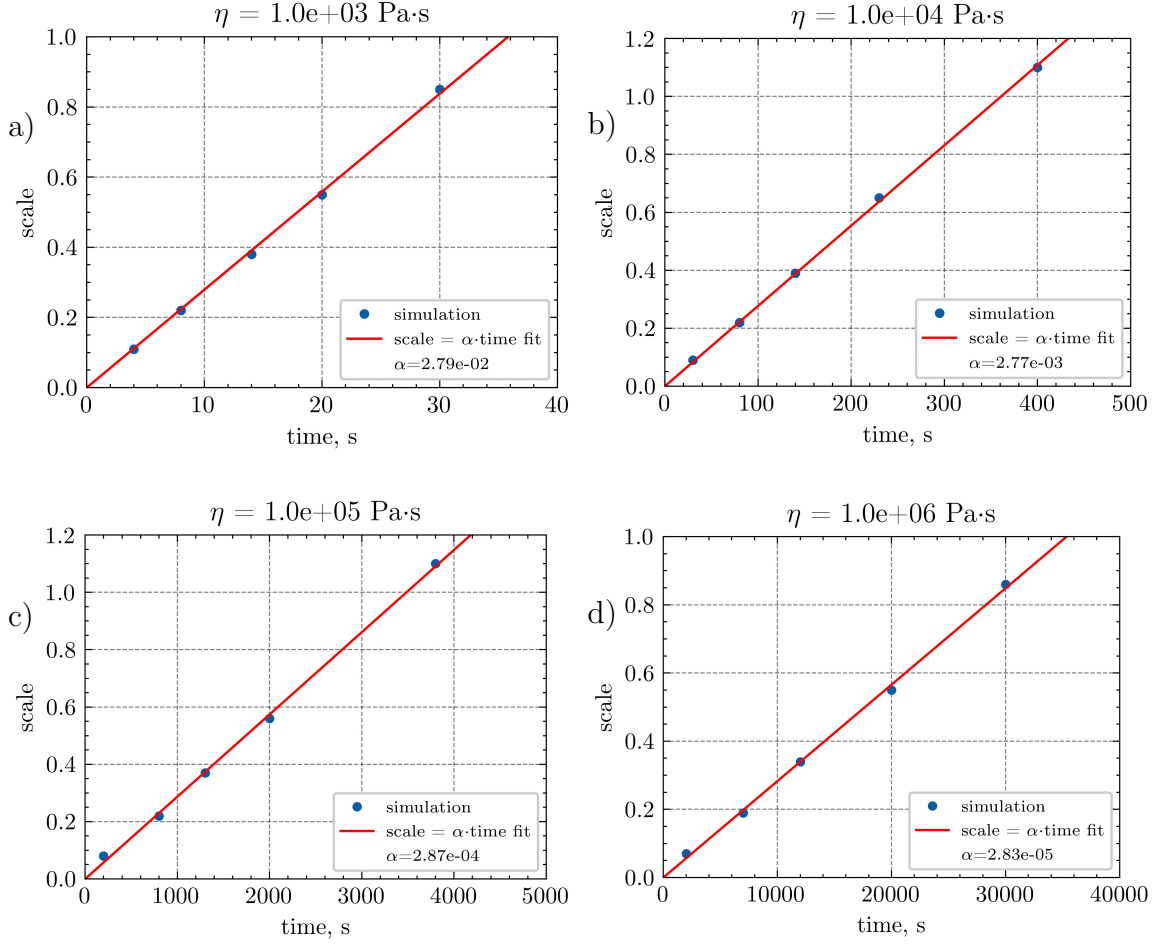


**Figure 7.** Time-scale dependencies for different viscosity values fitted with linear function.

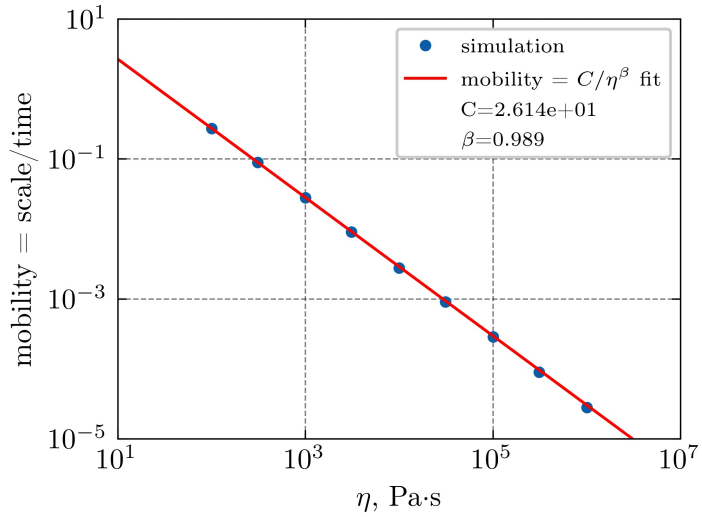


**Figure 8.** Linear fit of obtained dependence of  $\ln(\alpha)$  on  $\ln(\eta)$ .

by lithographic methods in PMMA. Indeed, in case of structures obtained by (grayscale) e-beam lithography any exposure profile can be converted into viscosity distribution by

solution of kinetic equations; in case of structures obtained by nanoimprint lithography only PMMA viscosity dependence on temperature and molecular weight should be taken into account. PMMA viscosity distribution is then directly converted into the mobility distribution of sample surface vertices. If sample size is much greater than structure period one can neglect the edge effects (contact angle etc.) during the reflow simulation far from sample edges. Then structure geometry and vertex mobility distribution become the only parameters required for simulation.

Third, the described algorithm allows to expand the boundaries of thermal reflow application. At present, thermal reflow is used predominantly for profile smoothing, which not causes dramatic profile transformation [1, 20]. This leads to sophisticated grayscale lithography process, which is mandatory for achievement of staircase profile close enough to required one. The complex but predictable reflow process in turn could simplify the whole fabrication method provided that greater part of profile is being formed by reflow.

## 5. Conclusion

The simulation technique for viscoelastic thermal reflow of structures obtained in PMMA with non-uniform viscosity profile is proposed. It bases on numerical search of minimal surface by finite elements method, processed by free software “Surface Evolver” (SE). Non-uniformity of resist is described by specific distribution of vertex mobilities of polymer surface, which is set in SE simulation processed in area normalization mode. For the determination of mobility distribution PMMA viscosity profile is calculated in two steps. First, Monte-Carlo algorithm is used for the simulation e-beam induced PMMA main-chain scissions during exposure. Then scission rate is calculated and used in kinetic equations, which describe changes in PMMA molecular weight distribution. The latter allows to calculate local number average PMMA molecular weight after exposure. Number average molecular weight is then used for calculation of PMMA viscosity profile at given temperature.

The relation between PMMA viscosity and vertex mobility of its surface was determined by simulation of rectangular grating reflow by two approaches – analytical, based on decay simulation of profile spatial harmonics and numerical one, processed by SE. The obtained agreement between reflowed profiles reveal linear dependence between SE scale factor and reflow time. Reflow simulation in wide viscosity range result in almost linear dependence of inverse mobility and viscosity. Using this relation, one can easily process SE reflow simulation with scale factor denoting actual reflow time.

The developed algorithm of vertex mobility calculation for e-beam exposed PMMA samples allows one to get a deep insight into non-uniform polymer reflow process. This can be used for simplification of complex 3D structure fabrication by wider application of thermal reflow processes.

## Appendix - Solution of moment equations

Moment equations

$$\frac{dM_i}{dt} = k_s \left( \frac{2}{i+1} - 1 \right) M_{i+1} + \frac{dM_0}{dt} - k_s M_1 - \frac{i}{\gamma} \left( k_s M_i + \frac{dM_{i-1}}{dt} \right) \quad (i \geq 1)$$

could be simplified by introduction of dimensionless variables (index “0” corresponds to initial value):

$$\begin{aligned}\tau &= y_0 k_s t, \\ \tilde{M}_1 &= M_1 / M_1^0, \\ \tilde{y} &= y / y_0, \\ \tilde{\gamma} &= \gamma y_0, \\ \tilde{x} &= x / x_0 = [y(z+1) / y_0(z_0+1)].\end{aligned}$$

Equations in form of (12) for  $i = 1, 2$  and  $3$  are then could be written as (here and further “SymPy” Python module was used for algebraic calculations):

$$\begin{aligned}&\frac{M_1^0}{\gamma(z(t)+1)^2 \tilde{y}^2(t)} \left[ -\gamma y_0 (z(t)+1)^2 \tilde{y}^2(t) \frac{d}{dt} \tilde{M}_1(t) (z(t)+1)^2 \tilde{M}_1(t) \tilde{y}^2(t) - \right. \\ &\quad \left. + (z(t)+1) \tilde{M}_1(t) \frac{d}{dt} \tilde{y}(t) - (z(t)+1) \tilde{y}(t) \frac{d}{dt} \tilde{M}_1(t) + \tilde{M}_1(t) \tilde{y}(t) \frac{d}{dt} z(t) \right] = 0, \\ &-\frac{M_1^0 y_0}{3\gamma} \left[ \gamma y_0 \left( (z(t)+2)(z(t)+3) \tilde{M}_1(t) \tilde{y}^2(t) + 3(z(t)+2) \tilde{M}_1(t) \frac{d}{dt} \tilde{y}(t) + \right. \right. \\ &\quad \left. \left. 3(z(t)+2) \tilde{y}(t) \frac{d}{dt} \tilde{M}_1(t) + 3\tilde{M}_1(t) \tilde{y}(t) \frac{d}{dt} z(t) \right) + 6(z(t)+2) \tilde{M}_1(t) \tilde{y}(t) + 6 \frac{d}{dt} \tilde{M}_1(t) \right] = 0,\end{aligned}$$

and

$$\begin{aligned}&-\frac{M_1^0 y_0^2}{2\gamma} \left[ \gamma y_0 \left( (z(t)+2)(z(t)+3)(z(t)+4) \tilde{M}_1(t) \tilde{y}^2(t) + \right. \right. \\ &\quad 4(z(t)+2)(z(t)+3) \tilde{M}_1(t) \frac{d}{dt} \tilde{y}(t) + \\ &\quad 2(z(t)+2)(z(t)+3) \tilde{y}(t) \frac{d}{dt} \tilde{M}_1(t) + 2(z(t)+2) \tilde{M}_1(t) \tilde{y}(t) \frac{d}{dt} z(t) + \\ &\quad \left. \left. 2(z(t)+3) \tilde{M}_1(t) \tilde{y}(t) \frac{d}{dt} z(t) \right) \tilde{y}(t) + \right. \\ &\quad 6(z(t)+2)(z(t)+3) \tilde{M}_1(t) \tilde{y}^2(t) + 6(z(t)+2) \tilde{M}_1(t) \frac{d}{dt} \tilde{y}(t) + \\ &\quad \left. \left. 6(z(t)+2) \tilde{y}(t) \frac{d}{dt} \tilde{M}_1(t) + 6\tilde{M}_1(t) \tilde{y}(t) \frac{d}{dt} z(t) \right] = 0,\right.\end{aligned}$$

The extracted expressions for derivations  $\tilde{M}_1$ ,  $\tilde{y}$  and  $\tilde{y}$  are

$$\begin{aligned}\frac{d\tilde{M}_1(t)}{d\tau} &= -\tilde{M}_1(t) \tilde{y}(t) \frac{A}{B}, \\ \frac{d\tilde{y}(t)}{d\tau} &= \tilde{y}^2(t) \frac{C}{6D},\end{aligned}$$

$$\frac{d\tilde{y}(t)}{d\tau} = -\gamma y^0 \tilde{y}^2(t) z(t) \frac{E}{F},$$

where

$$\begin{aligned}
A &= 9\gamma^2 (y^0)^2 \tilde{y}^2(t) z^3(t) + 41\gamma^2 (y^0)^2 \tilde{y}^2(t) z^2(t) + 58\gamma^2 (y^0)^2 \tilde{y}^2(t) z(t) + \\
&\quad 24\gamma^2 (y^0)^2 \tilde{y}^2(t) + 24\gamma y^0 \tilde{y}(t) z^2(t) + 96\gamma y^0 \tilde{y}(t) z(t) + 96\gamma y^0 \tilde{y}(t) + 36z(t) + 72, \\
B &= 6\gamma^3 (y^0)^3 \tilde{y}^3(t) z^3(t) + 24\gamma^3 (y^0)^3 \tilde{y}^3(t) z^2(t) + 30\gamma^3 (y^0)^3 \tilde{y}^3(t) z(t) + \\
&\quad 12\gamma^3 (y^0)^3 \tilde{y}^3(t) + 18\gamma^2 (y^0)^2 \tilde{y}^2(t) z^2(t) + \\
&\quad 66\gamma^2 (y^0)^2 \tilde{y}^2(t) z(t) + 60\gamma^2 (y^0)^2 \tilde{y}^2(t) + 36\gamma y^0 \tilde{y}(t) z(t) + 84\gamma y^0 \tilde{y}(t) + 36, \\
C &= \gamma^3 (y^0)^3 \tilde{y}^3(t) z^5(t) + 5\gamma^3 (y^0)^3 \tilde{y}^3(t) z^4(t) + 3\gamma^3 (y^0)^3 \tilde{y}^3(t) z^3(t) - \\
&\quad 17\gamma^3 (y^0)^3 \tilde{y}^3(t) z^2(t) - 28\gamma^3 (y^0)^3 \tilde{y}^3(t) z(t) - 12\gamma^3 (y^0)^3 \tilde{y}^3(t) + \\
&\quad 6\gamma^2 (y^0)^2 \tilde{y}^2(t) z^4(t) + 27\gamma^2 (y^0)^2 \tilde{y}^2(t) z^3(t) + 19\gamma^2 (y^0)^2 \tilde{y}^2(t) z^2(t) - \\
&\quad 52\gamma^2 (y^0)^2 \tilde{y}^2(t) z(t) - 60\gamma^2 (y^0)^2 \tilde{y}^2(t) + 18\gamma y^0 \tilde{y}(t) z^3(t) + 42\gamma y^0 \tilde{y}(t) z^2(t) - \\
&\quad 24\gamma y^0 \tilde{y}(t) z(t) - 84\gamma y^0 \tilde{y}(t) - 36, \\
D &= \gamma^3 (y^0)^3 \tilde{y}^3(t) z^3(t) + 4\gamma^3 (y^0)^3 \tilde{y}^3(t) z^2(t) + 5\gamma^3 (y^0)^3 \tilde{y}^3(t) z(t) + \\
&\quad 2\gamma^3 (y^0)^3 \tilde{y}^3(t) + 3\gamma^2 (y^0)^2 \tilde{y}^2(t) z^2(t) + 11\gamma^2 (y^0)^2 \tilde{y}^2(t) z(t) + \\
&\quad 10\gamma^2 (y^0)^2 \tilde{y}^2(t) + 6\gamma y^0 \tilde{y}(t) z(t) + 14\gamma y^0 \tilde{y}(t) + 6, \\
E &= \gamma^2 (y^0)^2 \tilde{y}^2(t) z^5(t) + 9\gamma^2 (y^0)^2 \tilde{y}^2(t) z^4(t) + \\
&\quad 31\gamma^2 (y^0)^2 \tilde{y}^2(t) z^3(t) + 51\gamma^2 (y^0)^2 \tilde{y}^2(t) z^2(t) + \\
&\quad 40\gamma^2 (y^0)^2 \tilde{y}^2(t) z(t) + 12\gamma^2 (y^0)^2 \tilde{y}^2(t) + \\
&\quad 6\gamma y^0 \tilde{y}(t) z^4(t) + 48\gamma y^0 \tilde{y}(t) z^3(t) + \\
&\quad 138\gamma y^0 \tilde{y}(t) z^2(t) + 168\gamma y^0 \tilde{y}(t) z(t) + \\
&\quad 72\gamma y^0 \tilde{y}(t) + 18z^3(t) + 84z^2(t) + 126z(t) + 60, \\
F &= 6\gamma^3 (y^0)^3 \tilde{y}^3(t) z^3(t) + 24\gamma^3 (y^0)^3 \tilde{y}^3(t) z^2(t) + \\
&\quad 30\gamma^3 (y^0)^3 \tilde{y}^3(t) z(t) + 12\gamma^3 (y^0)^3 \tilde{y}^3(t) + \\
&\quad 18\gamma^2 (y^0)^2 \tilde{y}^2(t) z^2(t) + 66\gamma^2 (y^0)^2 \tilde{y}^2(t) z(t) + \\
&\quad 60\gamma^2 (y^0)^2 \tilde{y}^2(t) + 36\gamma y^0 \tilde{y}(t) z(t) + 84\gamma y^0 \tilde{y}(t) + 36.
\end{aligned}$$

According original study [17] the solution of this equations was started by the Runge-Kutta method and continued by Hamming's predictor-corrector method.

## References

- [1] Robert Kirchner and Helmut Schift. “Thermal reflow of polymers for innovative and smart 3D structures: A review”. In: *Materials Science in Semiconductor Processing* 92.March (2019), pp. 58–72.
- [2] Arne Schleunitz et al. “Combining nanoimprint lithography and a molecular weight selective thermal reflow for the generation of mixed 3D structures”. In: *Journal of Vacuum Science & Technology B* 29.6 (2011), 06FC01.
- [3] T. Leveder, S. Landis, and L. Davoust. “Reflow dynamics of thin patterned viscous films”. In: *Applied Physics Letters* 92.1 (2008), pp. 90–93.
- [4] Tanguy Leveder et al. “Thin polymer films viscosity measurements from nanopatterning method”. In: *Journal of Vacuum Science & Technology B* 28.6 (2010), pp. 1251–1258.
- [5] T Leveder et al. “Reflow of supported sub-100 nm polymer films as a characterization process for NanoImprint lithography”. In: *Microelectronic Engineering* 88.8 (2011), pp. 1867–1870.
- [6] Robert Byron Bird, Robert Calvin Armstrong, and Ole Hassager. “Dynamics of polymeric liquids. Vol. 1: Fluid mechanics”. In: (1987).
- [7] Johanna Aho and Seppo Syrjälä. “On the measurement and modeling of viscosity of polymers at low temperatures”. In: *Polymer Testing* 27.1 (2008), pp. 35–40.
- [8] F Bueche. “Viscoelasticity of Poly Methacrylates”. In: *Journal of Applied Physics* 26.6 (1955), pp. 738–749.
- [9] Kenneth A. Brakke. “The Surface Evolver”. In: *Experimental Mathematics* 1.2 (1992), pp. 141–165.
- [10] Robert Phelan, Denis Weaire, and Kenneth Brakke. “Computation of Equilibrium Foam Structures Using the Surface Evolver”. In: *Experimental Mathematics* 4.3 (1995), pp. 181–192.
- [11] M. Jamali and H. Vahedi Tafreshi. “Numerical simulation of two-phase droplets on a curved surface using Surface Evolver”. In: *Colloids and Surfaces A: Physicochemical and Engineering Aspects* 629 (2021), p. 127418.
- [12] Robert Kirchner and Helmut Schift. “Mobility based 3D simulation of selective, viscoelastic polymer reflow using surface evolver Mobility based 3D simulation of selective, viscoelastic polymer reflow”. In: *Journal of Vacuum Science & Technology B* 32.6 (2014), 06F701.
- [13] Robert Kirchner, Arne Schleunitz, and Helmut Schift. “Energy-based thermal reflow simulation for 3D polymer shape prediction using Surface Evolver”. In: *Journal of Micromechanics and Microengineering* 24 (2014), 055010 (7pp).
- [14] F Sidorov et al. “Direct Monte-Carlo simulation of dry e-beam etching of resist”. In: *Microelectronic Engineering* 227 (2020), p. 111313.

- [15] Richard H. Boyd. "Theoretical Depolymerization Kinetics in Polymers Having an Initial "Most Probable" Molecular Weight Distribution". In: *Journal of Chemical Physics* 31.2 (1959), pp. 321–328.
- [16] Richard H. Boyd and Tungpo Lin. "Theoretical Depolymerization Kinetics. II. The Effect of Molecular-Weight Distribution in Degrading Polymers Undergoing End-Group Initiation". In: *Journal of Chemical Physics* 45.3 (1966), pp. 773–777.
- [17] Richard H. Boyd and Tung-Po Lin. "Theoretical Depolymerization Kinetics. III. The Effect of Molecular-Weight Distribution in Degrading Polymers Undergoing Random-Sission Initiation". In: *Journal of Chemical Physics* 45.3 (1966), pp. 778–781.
- [18] A. M. Kotliar. "Evaluation of molecular weight averages resulting from random chain scission process for wide distributions as in polyolefins". In: *Journal of Polymer Science Part A: General Papers* 2.3 (1964), pp. 1057–1067.
- [19] Itaru Mita, Kazuhito Obata, and Kazuyuki Horie. "Photoinitiated Thermal Degradation of Polymers II. Poly(methyl methacrylate)". In: *Polymer Journal* 22.5 (1990), pp. 397–410.
- [20] Robert Kirchner et al. "How post-processing by selective thermal reflow can reduce the roughness of 3D lithography in micro-optical lenses". In: *Laser 3D Manufacturing IV*. Vol. 10095. SPIE. 2017, pp. 8–16.